SLAC-PUB-95-6773

Magnetism with Picosecond Field Pulses†

H.C. Siegmann*, E.L. Garwin, C.Y. Prescott
Stanford Linear Accelerator Center, Stanford University, Stanford, CA 94309

J. Heidmann[1], D. Mauri[2], D. Weller[2]
[1] *IBM Storage Systems Division, 5600 Cottle Road, San Jose, CA 95193*
[2] *IBM Research Division, Almaden Research Center, 650 Harry Road, San Jose, CA 95120*

R. Allenspach, W. Weber
IBM Research Division, Zurich Research Laboratory, CH-8803 Rüschlikon, Switzerland

Ultrashort magnetic field pulses of 6 ps duration surrounding the focus of 50 GeV electron bunches are shown to write a magnetic pattern into both perpendicular and in-plane metallic magnetic recording films. High-resolution magnetic contrast images allow the distinction between an immediate writing process governed by coherent rotation while the beam field is present and a thermomagnetic process wherever the material is heated close to the Curie point.

(Submitted to Physical Review Letters)

†This work was supported in part by the Department of Energy under contract DE-AC03-76SF00515

*On sabbatical leave from the Swiss Federal Institute of Technology, Zürich.

Research on the time dependence of magnetization processes has been limited to the nanosecond time scale because magnetic field pulses with a duration of picoseconds could not be made [1]. However, the pulsed electron beams of $\approx 10^3$A accelerated to 50 GeV at the Stanford linear accelerator can be squeezed through a focus of $\approx 1\ \mu\text{m}^2$ cross section generating a unique magnetic field pulse in the laboratory frame [2]. The magnetic field pulse combines short duration with strength that can reach the Megagauss range on approaching the surface of the beam.

We show here that this magnetic field pulse writes a magnetic pattern into thin-film magnetic recording media. The pattern can be read long after the beam has passed. Hence a wealth of new magnetic studies is possible combining the current densities of 10^{15} A/m^2 produced by electron accelerators with the recent advances in fabricating thin magnetic structures, and in imaging the magnetic patterns with unprecedented spatial resolution. The familiar rotation model assumes that the magnetization $\vec{M}$ precesses as a whole around the magnetic field. We show that this model can describe the reversal as well as the rotation of $\vec{M}$ into the field direction induced by the beam field $\vec{H}_\mathrm{B}$ in thin magnetic films. A single magnetic field pulse of 6 ps duration is sufficient to reverse $\vec{M}$ if $\vec{H}_\mathrm{B}$ is applied perpendicularly. We find a spread of the reversal transition over an area having widely varying strengths of $\vec{H}_\mathrm{B}$. Such fluctuations are likely to be relevant to the still unsolved problem of magnetization reversal in simple uniaxial systems [3].

$\vec{H}_\mathrm{B}$ can readily penetrate into the metallic films because the latter are in thickness less than 1/10 of the classical skin depth for a rise time of 10^{-12} s. Yet the electric field of the beam is screened on the femtosecond time scale and will be neglected.

At the final focus test beam (FFTB) facility of the Stanford Linear Accelerator, the electron beam density distribution $n(x, y, z)$ can be approximated by a Gaussian in three coordinates, where $\sigma_x = 3.5\ \mu$m, $\sigma_y = 0.2\ \mu$m, $\sigma_z = 0.9$ mm, and z is the beam direction. The history plot of the beam flux shows that the total number of electrons was $N = \int\int\int n(x, y, z)dx\,dy\,dz = 6{\cdot}10^9$ during the present experiment.

In the near-field region of interest here, the magnetic field $\vec{H}_\mathrm{B}(x, y)$ is calculated from the current density $j(x, y, t) = n(x, y, t) \cdot e \cdot c$ using Ampère's law, where e is the elementary charge, c the speed of light, and the time is $t = -z/c$. The maximum instantaneous field strength occurs at $t = 0$. In the discussion, we assume for simplicity a square field pulse of duration $\tau = 2\sigma_z/c = (6 \pm 1)$ ps and maximum field amplitude [4].

In the first set of experiments, $Co_{28}Pt_{72}$ alloy films with perpendicular remanent magnetization were used. These materials have been developed for thermomagnetic writing in magneto-optic storage disks [5,6]. The particular structure we examine in the following consists of a 16-nm-thick polycrystalline $Co_{28}Pt_{72}$ alloy film which was coevaporated at 220 °C onto a 20-nm-thick fcc (111) Pt seed layer on a fused silica platelet of 500 μm thickness and capped with 2 nm Pt against corrosion. It showed an almost perfectly square hysteresis with a measured perpendicular remanence of 99.5% at room temperature. The premagnetized samples were mounted on an open rectangular holder, which was then translated by a stepping motor across the focus in the FFTB facility. Each sample was exposed to either one or two electron pulses impinging along the surface normal. After exposure, the entire rectangular structure was withdrawn from the beam and recovered many weeks later for microscopic inspection.

A wide-field Kerr microscope has been used for imaging the written magnetic structures. The microscope was set up to be sensitive to the polar magneto-optic Kerr effect using white light for illumination [7]. Fig. 1 shows the location of impact of a single electron pulse. Four different regions can be distinguished. A: The outer region where the magnetization M^- is unchanged (the graded contrast is an artifact due to inhomogeneous illumination). B: The "elliptic" region where M^- has switched to M^+. C: The bar-like region with a sharp boundary where M^+ is again inverted. D: The center with a small rim. The line scan in Fig. 1 taken along the y-axis at $x = 0$ shows the spatial extent of the various regions. In region D, the material has evaporated and melted and there is no more magnetization. In C, the material was heated to temperatures $T > T_\mathrm{C}$, where $T_\mathrm{C} \cong 300$ °C is the Curie point. Upon cooling in the dipolar field of the surrounding magnetized material, a reversed domain is formed corresponding to a thermomagnetic writing process. However, the Kerr signal change in the transition B$\rightarrow$C is smaller than in A$\rightarrow$B. This indicates that some perpendicular remanence was lost, probably due to overheating. The extension of region C up to $x \cong 20\ \mu$m cannot be due to heat diffusing from the main focus, as diffusion would generate a shape resembling a circle at these distances. There has to be some additional source of heat, generated for example by a slower-than-Gaussian falloff of the beam density at large distances from the focus. Such halos at or even below the 1% intensity level are sufficient to account for the heating of region C.

Regions C and D are formed by the interaction of the high-energy electron beams. The energy density initially generated in material of density ρ by a beam pulse of cross section s is $q = (N\epsilon\rho)/s$, where $\epsilon = 3.5 \times 10^{-13}$ (Joule cm^2)/g·electron). With Pt, q is 20 times the heat of vaporization. Yet the energy propagating into the material from the focus is reduced by energy loss due to the emission of bremsstrahlung, thermal radiation, secondary electrons, evaporation of atoms, and heat conduction into the substrate in which one-tenth of the initial energy is deposited due to its lower density. However, at any location away from the focus, $\vec{H}_B$ arrives long before the heat wave. Even the energy transported by the supersonic shock wave reaches $y = 1$ μm only after 10^3 ps, whereas transport via regular heat conduction takes 10^6 ps. This shows that the magnetization processes induced by $\vec{H}_B$ at large distances and outside the halo take place in undisturbed material at ambient temperature.

We focus in this paper on the magnetization reversals along $x = 0$ from A→B and B→C. First we note that transition A→B is fuzzy whereas B→C is sharp. Small domains are identified in the transition A→B. The reversed domains retain their width but are separated by increasingly wide nonreversed regions upon moving from the midpoint of the reversal to larger distances. At the midpoint of the reversal, half of the domains are up and half down. This occurs at $x = 0$, $y = 14$ μm. We note that the contour line of constant magnetic field pulse amplitude H_B = const. passing through that point does not follow the observed shape of the reversal. The pointed edge at $x = 20$ μm, $y = 0$ would require $\sigma_x = 8$ μm (instead of the actual $\sigma_x = 3.5$ μm). Increased temperature while $\vec{H}_B$ is acting results in the outward shift of the reversal because the magnetic anisotropy decreases with increasing T. We therefore confine the interpretation to the line $x = 0$.

The magnetic anisotropy field $\vec{H}_A$ is defined as the field needed to saturate the sample in the hard plane. We determined in separate experiments that $H_A = 1600 \pm 100$ kA/m at room temperature. To rigorously test the rotation model, the Landau–Lifshitz equation [8] must be solved which is beyond the scope of the present paper. However, neglecting the damping term, assuming pure spin moments, and a square field pulse simplifies the problem greatly, and yields $H_B^* \cong H_A$ for the amplitude of the field pulse inducing the reversal in the present material in 6 psec. This is valid for the midpoint of the reversal which is determined by the condition that $\vec{M}$ must precess into the hard plane while $\vec{H}_B$ lasts. From the hard plane, $\vec{M}$ can relax in due time into either one of the two easy directions.

The field strength at $x = 0$, $y = 14$ μm satisfies this condition within the present experimental uncertainty (mainly given by the uncertainty of σ_z). Therefore, the location of the reversal transition is consistent with the rotation model. Additional results obtained with five different samples with thicknesses ranging from 8 to 16 nm and H_A from 1360 to 1760 kA/m all showed that the midpoint of the reversal occurs at $H_A \cong H_B$ along $x = 0$.

However, the additional result going beyond the rotation model is that the reversal occurs over a width of $\Delta y = 4$ μm. This leads to a relative spread of the switching field of $\Delta H_B^*/H_B^* = \Delta y/y = \pm 30\%$. This must be due to locally variable angular velocities of $\vec{M}$, which in turn leads to a situation at the end of the beam pulse where $\vec{M}$ has transcended the hard plane in some locations but not in others. The subsequent relaxation of $\vec{M}$ into the nearest easy direction generates domains. The phenomenon might be explained by fluctuations of the anisotropy due to crystal defects. Yet because the duration of $\vec{H}_B$ is of the order of the phonon frequencies, fluctuations of the anisotropy could also be thermally excited. Further experiments in which the temperature is varied may verify which of these two possibilities is valid. It is interesting to note that the width of a magnetic domain wall is 1000 times smaller than the width of the reversal induced by $\vec{H}_B$.

The pattern generated by two consecutive electron pulses separated by 1 s is shown in Fig. 2. It confirms the above interpretations. The center region D is similar to the one of a single pulse. Yet the thermomagnetic region C must always be magnetized opposite to the surrounding material. We see that M^- has indeed switched to M^+. In the inner part of region B, the magnetization M^+ is reversed again to the initial direction M^- prior to the first pulse. This is also expected because a second reversal merely produces the initial state. Yet the interesting fact is that a stripe having some domains of M^+ is left. At $x = 0$, the stripe is centered at $y = \pm 14$ μm, which is the midpoint where $M^+/M^- = 1$ after the first pulse. During the second pulse, both M^+ and M^- precess again into the hard plane, from which they relax into either M^+ or M^- with equal probability. Therefore, the midpoint of the reversal $M^+/M^- = 1$ must remain stationary as observed.

The second type of magnetic material was a CoPtCr alloy developed for high-density in-plane magnetic recording [9]. This material features an isotropic easy plane coinciding with the plane of the film and a hard axis perpendicular to it. The coercivity is $H_c = 64$ kA/m, and the in-plane remanence is 87% of the saturation independent of the direction in which the external field is applied within the film plane. A film of 38-nm thickness was deposited directly onto a 250-μm-thick Si(100) wafer having no extra capping.

Fig. 3 shows such an in-plane sample that was struck by 30 consecutive electron pulses at a rate of 1 pulse per second. The pictures are taken with spin-polarized scanning electron microscopy (spin-SEM) after the surface had been cleaned by mild sputtering. In spin-SEM, low-energy secondary electrons are excited by focusing a primary electron beam onto the surface of the sample. Topographic contrast results from the intensity of the secondaries, whereas their spin polarization yields the magnetization of the surface layers [10,11]. The upper part of Fig. 3 is topographic and shows the location of impact of the 50 GeV electron beam and the small extent of its material damage. The lower picture displays the direction of the secondary electron spin polarization, i.e. the magnetization direction in each location. The sample had been premagnetized along the line $x = y$ prior to exposure, with the x direction again parallel to the long axis of the pulse induced structure. We see that the boundaries of the magnetic pattern generated by the electron pulses are as large as $86 \times 105\ \mu m^2$. There are two whorls in the x-direction $\approx 45\ \mu m$ apart. Studying the magnetization generated by 1, 3, 10 and 30 pulses, we arrived at the following model explaining how an initial angle of φ between $\vec{M}$ and $\vec{H}_B$ decreases asymptotically to $\varphi \rightarrow 0$ with each electron pulse: When $\vec{H}_B$ is switched on, $\vec{M}$ precesses around $\vec{H}_B$, building up a perpendicular component $M_\perp$. This in turn generates a demagnetizing field $H_z = -(1/\mu_0)M_\perp$. $\vec{M}$ now precesses around H_z as well, thereby turning in the direction of $\vec{H}_B$. After $\vec{H}_B$ is switched off, $\vec{M}$ relaxes into the plane of the film, which reduces φ except in the rare cases where the precession angle is a multiple of π. Therefore, each electron pulse adds to the circular magnetization along the beam field $\vec{H}_B$. This is in contrast to the perpendicular samples, where the even pulses reverse what the odd pulses have generated.

This model does not explain the two whorls. From the experiments with the perpendicular samples, we know that these whorls are located just at the boundaries where the material is heated to $T \geq 300$ °C. Because the coercivity approaches 0 at 400 °C, we suspect that the whorls are a thermomagnetic feature arising in the stray field of the circular magnetization generated by $\vec{H}_B$.

In conclusion, we have shown that the magnetization $\vec{M}$ of thin magnetic structures responds to magnetic field pulses of 6 ps duration. The magnetic pattern imaged after a long time can be understood by coherent rotation of $\vec{M}$ while the beam field $\vec{H}_B$ is switched on, and subsequent relaxation into the nearest easy direction or plane.

We thank R.L. White, Center for Research on Information Storage Materials, Stanford University, for supporting this project. We gratefully acknowledge the advice and professional support received from a number of people, particularly the staff of the FFTB, as well as A. Carl, G.J. Collet, C. Field, and F. King. This work was supported in part by the Department of Energy under contract DE-AC03-76SF00515.

[1] Magnetic field pulses of 50 ps duration and 10 Gauss amplitude have been applied to the study of spin relaxation in EuS, see M.R. Freeman, R.R. Ruf, and R.J. Gambino, IEEE Trans. Mag. **27**, 4840 (1991).

[2] Physics Today, July 1994, p.22, and H.C. Siegmann and E.L. Garwin, *Magnetism with ultrashort magnetic field pulses from the SLAC FFTB*, SLAC Proposal (1994), unpublished, and references cited therein.

[3] M. Ledermann, S. Schultz, M. Ozaki, Phys. Rev. Lett. **73**, 1986 (1994).

[4] σ_x is experimentally determined from the width of the luminous region obtained in Stanford's Large Detector (SLD). However, SLD was not running during the present experiment, which is why the absolute value of σ_x is not well established here.

[5] D. Weller et al., Optical Memory and Neural Networks **3**, 353 (1994).

[6] D. Weller et al., Appl. Phys. Lett. **61**, 2726 (1992)

[7] W. Rave, R. Schäfer, A. Hubert, J. Magn. Magn. Mat. **65**, 7 (1987).

[8] L. Landau and E. Lifshitz, Phys. Z. Sowjetunion **8**, 135 (1935).

[9] Tadashi Yogi et al., IEEE Trans. Mag. **26**, 2271 (1990).

[10] H. Matsuyama and K. Koike, Rev.Sci.Instr. **62**, 970 (1991).

[11] R. Allenspach, J. Magn. Magn. Mater. **129**, 160 (1994).

FIG. 1. Magnetic pattern generated by a single electron pulse in a perpendicular $Co_{28}Pt_{72}$ alloy film. The x-axis is vertical. The line scan along $x = 0$ displays the polar Kerr signal obtained in a wide-field Kerr microscope. It is proportional to the component of the magnetization along the normal of the film. This interpretation of the signal is not valid in the center region where the material has melted or even evaporated, and no longer exhibits perpendicular magnetization.

FIG. 2. Magnetic pattern generated by two consecutive electron pulses separated by 1 s. Otherwise same as Fig. 1.

FIG. 3. Magnetic pattern of CoPtCr in-plane magnetic alloy generated by 30 consecutive electron pulses at a rate of 1 pulse/s. The data are taken by spin-SEM. Top: topography; bottom: in-plane magnetization direction indicated by arrows deduced from the images of both in-plane magnetization components. The magnetization component along the page (direction $x = -y$) is indicated by the color map. The sample has been premagnetized along $x = y$. Since the remanence is smaller than the saturation magnetization some small domains are also visible in the region which was not influenced by the electron pulse. Scan area: 148 μm $\times$ 148 μm. Bottom: Topography.

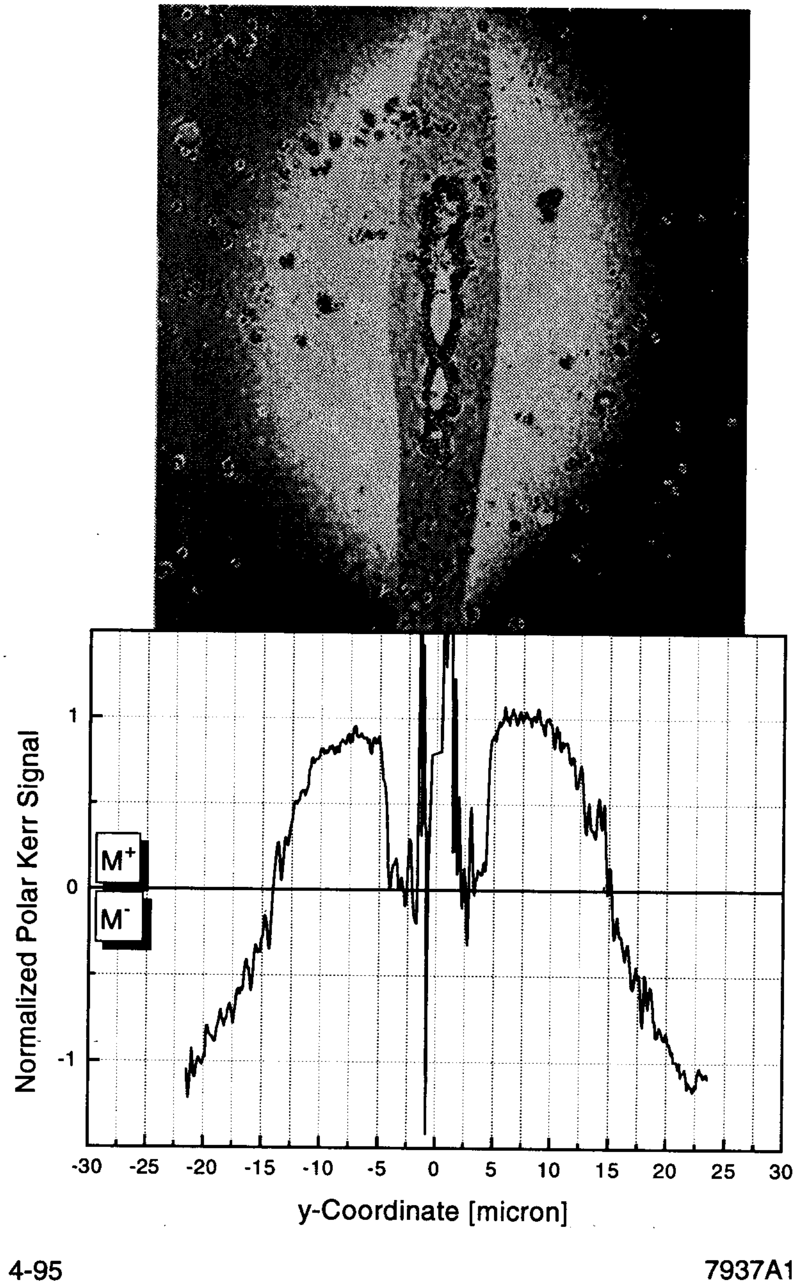
Normalized Polar Kerr Signal
1
0
-1
M+
M-
-30
-25
-20
-15
-10
-5
0
5
10
15
20
25
30
y-Coordinate [micron]
4-95
7937A1

Fig. 1

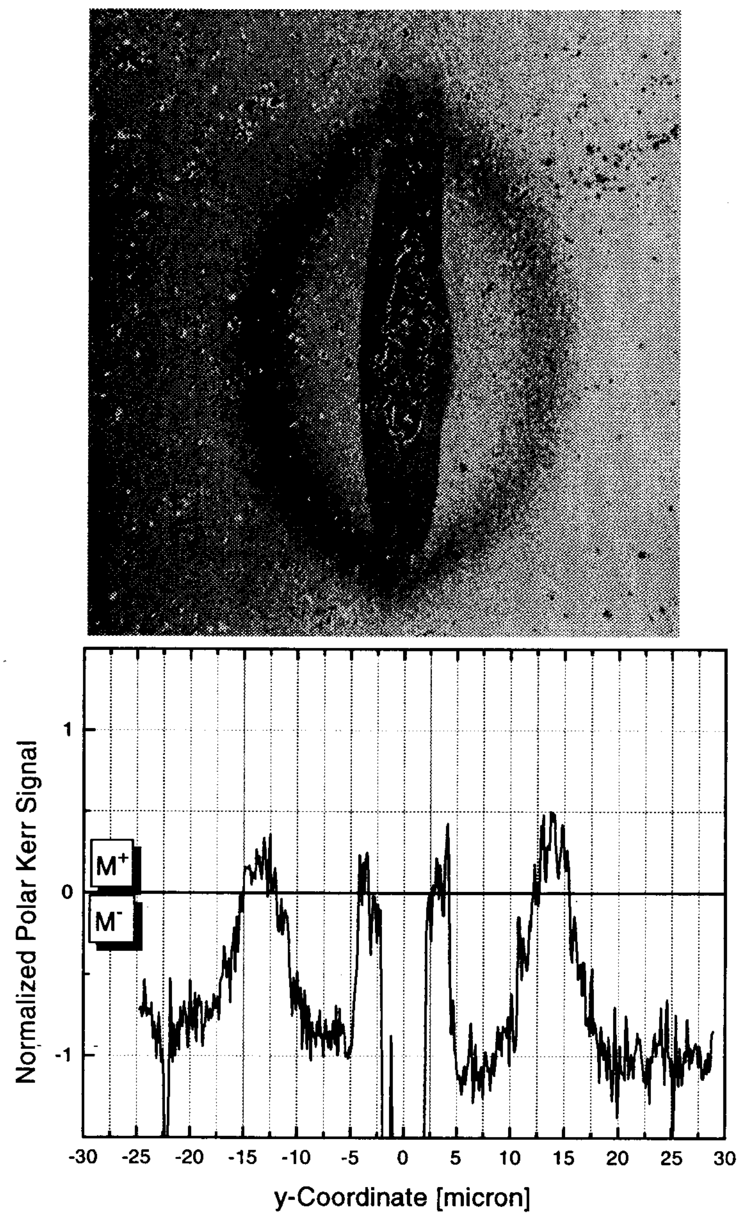

4-95 7937A2

Fig. 2

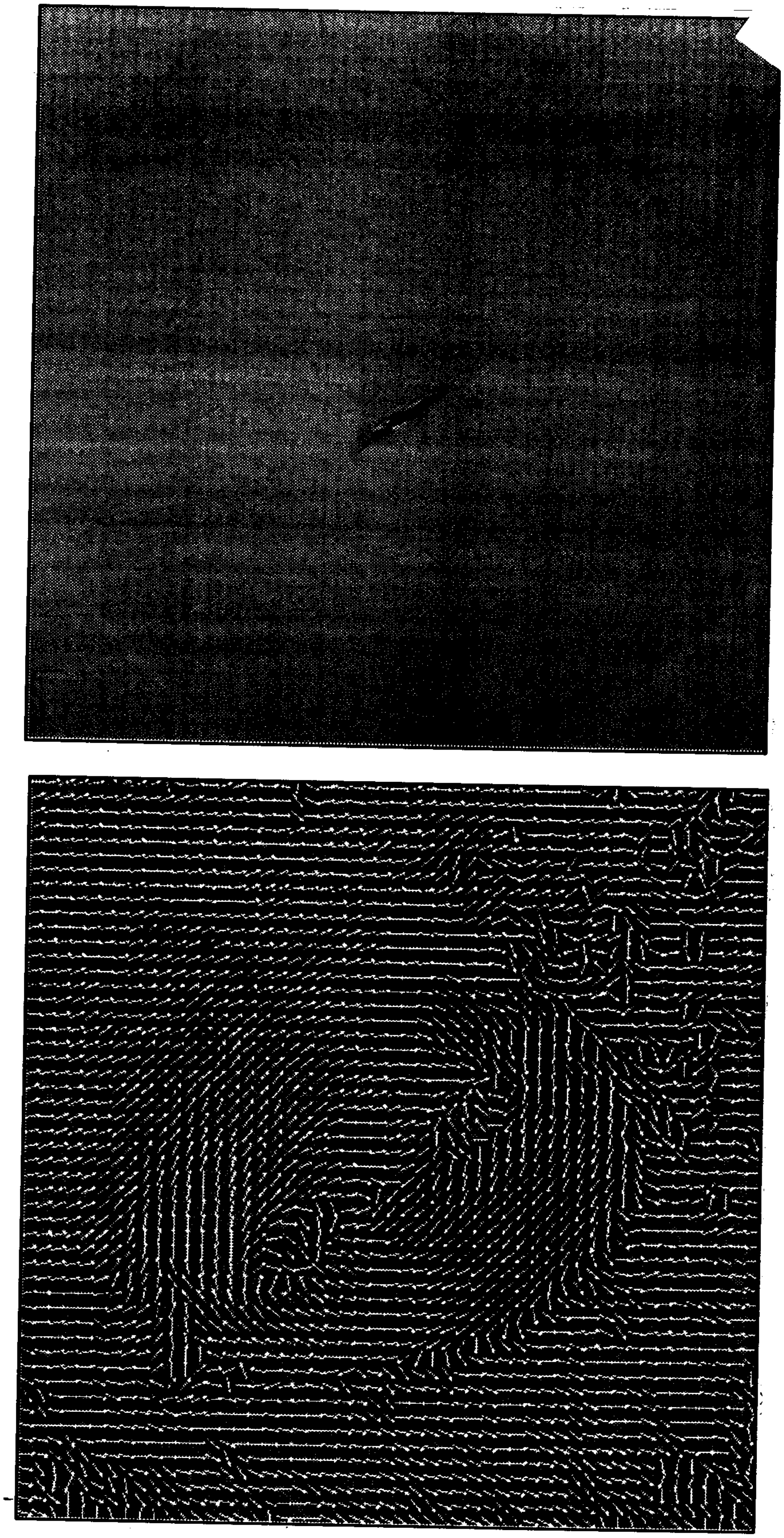

4-95

7937A3

Fig. 3